2037

NRL Report 6121

Structure in Textured Gold Films

J. E. Davey and R. H. Deiter

Solid State Electronics Branch
Electronics Division

September 4, 1964

APPROVED FOR PUBLIC
RELEASE - DISTRIBUTION
UNLIMITED

U.S. NAVAL RESEARCH LABORATORY
Washington, D.C.

CONTENTS

Abstract	ii
Problem Status	ii
Authorization	ii
INTRODUCTION	1
EXPERIMENTAL PROCEDURES	2
FILM STRUCTURE	3
Electron Diffraction Observations	3
X-Ray Diffraction Observations	3
Resistivity Measurements	8
DISCUSSION	9
ACKNOWLEDGMENT	16
REFERENCES	16

Copies available from Office of Technical Services
Department of Commerce – $.50

ABSTRACT

Gold films deposited by evaporation onto amorphous substrates at a wide variety of temperatures have been examined by x-ray and electron-reflection diffraction, as well as by resistivity measurements. It was found that: (a) the [111] texture predominates at all deposition temperatures and appears almost exclusively between 370° and 500° C; (b) the hexagonal partial structure, first noted by others in cold-worked bulk gold, appears in electron diffraction in this temperature range, along with the forbidden (110) reflection; (c) the deposition process introduces large concentrations of vacancies, which cluster under annealing into quite stable complexes. A large observed increase in resistivity and a contraction of the lattice as measured by x-ray diffraction are related to these vacancies.

PROBLEM STATUS

This is a final report on one phase of the project; work on other phases is continuing.

AUTHORIZATION

NRL Problem R08-35
Project RR 008-03-46-5658

Manuscript submitted May 18, 1964.

STRUCTURE IN TEXTURED GOLD FILMS

INTRODUCTION

Structure in gold films has been of interest since the early work (1935) of Finch, Quarrel, and Wilman (1), who observed anomalous structure occurring in reflection-diffraction photographs. This observation was at that time attributed to a solid solution of gas in the superficial layers of the electrodeposited films. In 1955 Hirsch, et al. (2) interpreted extra rings in beaten gold foils as due to a hexagonal close-packed (hcp) structure. Likewise, Bahadur and Sastry in 1961 (3) observed equivalent rings in gold films vacuum-deposited onto single-crystal rocksalt. Ogawa, et al. (4) also reported observing twinned layers in thin films of face-centered cubic (fcc) metals vacuum-deposited onto rocksalt. However, other workers (5,6) who have studied metal films deposited onto neutral substrates did not report finding extra reflections.

In the case of silver films deposited onto and stripped from rocksalt crystals, Goche and Wilman in 1939 (7) found extra reflections which they related to curvature inherent in the substrate surface and/or caused by the mechanical deformation associated with stripping the film from the single-crystal host. Burbank and Heidenreich in 1960 (8) observed extra reflections in nickel-iron alloys and interpreted these as due to double diffraction at {111} twin boundaries. Their interpretation involves the assumption that deformation of the film (buckling due to stripping) spreads the reciprocal lattice points, allowing intersection with the sphere of reflection. In a recent (1963) comprehensive work on gold films, Pashley and Stowell (9) invoked the double-diffraction argument to explain the extra reflections observed by earlier workers, who identified them with an hcp phase; in addition, Pashley and Stowell explained other previously unobserved spots as due to double diffraction at imperfect double-positioning boundaries. They also cite film buckling as a principal condition for observing the extra lines and spots.

In the present work, the structural properties of gold films deposited on neutral substrates have been investigated, using a combination of reflection-electron-diffraction and x-ray-diffraction techniques for the structural evaluation. With this method the film did not have to be stripped from the substrate; associated "cold-work" effects and buckling in the film were thereby eliminated. Since vacuum-deposited films may be expected to contain large concentrations of defects, especially when deposited at low temperatures, the properties of gold films deposited over a wide range of temperatures were investigated, and the effects of annealing on the structure of these films were examined. In addition, films were deposited on substrates with a variety of expansion coefficients, to eliminate strain-related structural effects (10,11). In the case of reflection diffraction on these films, the normal fcc structure in a textured state was observed, and, under particular conditions of deposition, the extra lines indexed by Hirsch, et al., as hcp reflections were noted. A previously unreported weak reflection inside the (111) ring was perceived, which has been tentatively identified as the forbidden (110); in no case was the inner of the two "$(111)^-$" rings inside the (111) ring detected. These rings were interpreted by Pashley and Stowell (9) as due to double-diffraction phenomena. In no case did x-ray measurements yield the forbidden (110), or lines characteristic of the hcp structure. However, the x-ray measurements did show Bragg-line shifts, which were associated with large concentrations of stable complexes of vacancies; these shifts are related to other observations on gold and other fcc metals (12,13,14).

EXPERIMENTAL PROCEDURES

The gold films were deposited for the most part in a commercial vacuum evaporator at pressures between 8×10^{-6} and 2×10^{-5} torr; however, other evaporations were performed in a Vac-Ion ultra-high-vacuum system. The substrate oven was of cylindrical quartz, heated indirectly with a close-wound helix of 20-mil tantalum wire. The oven was heat shielded with concentric cylinders of sheet tantalum. A tantalum shutter with a small hole was interposed between the evaporation source and the oven; by evaporating through this hole, radiation effects at the substrate were minimized, and evaporations could be carried out at substrate temperatures as low as 35°C. A total of about 100 films was evaporated, at temperatures between 35° and 750°C.

The substrates investigated were Pyrex, soda-lime glass, Nonex, fused quartz, polished Al_2O_3, and carbon films evaporated onto quartz and mica substrates. The technique of using an evaporated film of carbon (usually about 300 Å thick) on either quartz or mica was employed to preclude the effects of impurity contamination and/or ordering effects from the substrate, and also to provide values of expansion coefficient intermediate to the values characteristic of the glasses listed above. The overall range of coefficient was from $0.256 \times 10^{-6}/°C$ for quartz to $3.6 \times 10^{-5}/°C$ for muscovite mica. In addition, in connection with the annealing studies, the Bragg reflections from the mica were used for a secondary reference for determining the shift of the peak in gold films. That is, mica substrates were chosen such that one or more strong, well-defined Bragg reflections occurred in the forward reflection region. Such samples were used for the carbon evaporation, and then for the gold evaporation onto the carbon. With subsequent annealing, relative shifts of the Bragg reflections from the gold films could be referred to the unchanging Bragg reflections from the mica; such a technique is independent of absolute alignment of the x-ray equipment.

The evaporators were coils or boats of tungsten, tantalum, or molybdenum, or indirectly heated quartz cones; all components were given rigorous chemical cleaning. The evaporation rate was customarily about 30 Å/min; however, "flash evaporations" of about 500 Å/sec were also investigated. The low evaporation rates were used principally to minimize contamination from the evaporators (15). Normally the geometry of the gold deposit was such that all but the ends of the substrate was deposited upon. This procedure was found necessary, since in reflection electron diffraction the superimposed diffuse background from a section of bare substrate would tend to obscure the coherent diffraction from the gold film and make very weak reflections difficult, if not impossible, to observe. In addition, it has been found (16,17) that residual contaminants on substrate surfaces may provide an ordered low-intensity diffraction pattern which would appear inside the (111) ring for gold and confuse the structural observations pertaining to the gold films themselves.

The alignment of the GE XRD-3 spectrogoniometer was checked before and after each series of measurements with a gold film used as an absolute reference. This gold film was deposited on a quartz substrate and then annealed for five minutes at or above 1065°C, causing the film to melt and "ball up;" the anneal as the film returns to room temperature guarantees a vacancy-free structure with well-defined Bragg lines. The geometry of the film and substrate is such that for a well-aligned goniometer, the gold film not only is an optical flat but is directly on the focusing circle to within film thickness.

Resistivity measurements were made by conventional four-probe methods immediately after deposition and again before and after any annealing treatment. Film thickness was determined by photographing the interference fringes of the film in a Zeiss interferometer, enlarging the photographs, and measuring the fringe shift with a toolmaker's microscope.

FILM STRUCTURE

Electron Diffraction Observations

Films deposited at ambient temperature (i.e., with no current applied to the oven and the substrate heated only by radiation through the hole in the shutter) were found to have diffuse rings and to have a weak [111] texture. This behavior was observed for deposition temperatures ranging from about 35° to 125°C; for films deposited in this temperature range no extra lines were observable. For substrate temperatures above about 150°C, the [111] texture becomes well defined, and for deposition temperatures between 370° and 500°C a very strong [111] texture, with excellent particle size, was observed; in this temperature range extra lines, which could not be indexed according to the cubic structure, were also seen. A diffraction pattern typical of deposition in this temperature range is shown in Fig. 1. Since weak lines observed in such patterns may be lost in reproduction, a line drawing of all reflections observed in such patterns is also given in the figure; in addition a list of the normal cubic reflections is included. The extra lines are indexed, for convenience, in the hexagonal system, with the exception of the forbidden (110). While the (110) is quite weak and difficult to observe, it was seen for practically all depositions in the temperature range from 370° to 500°C; however, no line which could be indexed as $(111)^{-}$ was ever observed (9). On the other hand, the extra lines indexed as hexagonal in Fig. 1 were observed practically without exception at these temperatures; the $(10\bar{1}0)$ was always very well defined. The extra lines appear in diffraction patterns for films deposited up to temperatures as high as 650°C. For depositions much above 650°C, the extra lines begin to disappear; in addition, the [111] texture begins to weaken, and the diffraction patterns indicate large random particle growth. Diffraction patterns characteristic of the low-temperature and high-temperature deposition ranges are shown in Fig. 2a and Fig. 2b, respectively.

The results of observations made by reflection diffraction over the entire temperature range of deposition were found to be independent of the evaporator used, of the film-substrate mismatch in expansion coefficient, and of the evaporation rate, up to "flash evaporations" of 500 Å/sec. It is emphasized that the appearance of the extra lines did not have a critical enough dependence on any of these parameters to be observed by reflection diffraction.

It is to be noted that for depositions at about 400°C and above, the external surface of the film begins to take on a diffusely reflecting or matte appearance. This behavior becomes more pronounced with increasing temperature of deposition, yet it could not be related to the appearance of the extra lines in the diffraction patterns.

X-Ray Diffraction Observations

In the initial part of the present work, it was found that not all the films yielded resistivity values consistent with expected bulk behavior, and in addition that deviations from expected Bragg-line positions occurred. In view of work relating resistivity variations in thin films to the existence of twins and stacking faults (18,19) and of the authors' observations on the appearance of the extra lines in electron diffraction, it was concluded that it might be possible to correlate these effects with the Bragg-line shifts, associated with stacking faults and twinning in fcc metals. This relationship was reviewed by Warren in 1959 (20). Thus, extreme care had to be employed in the alignment of the spectrogoniometer. For the work reported here the highest-resolution slits available for this machine were employed.

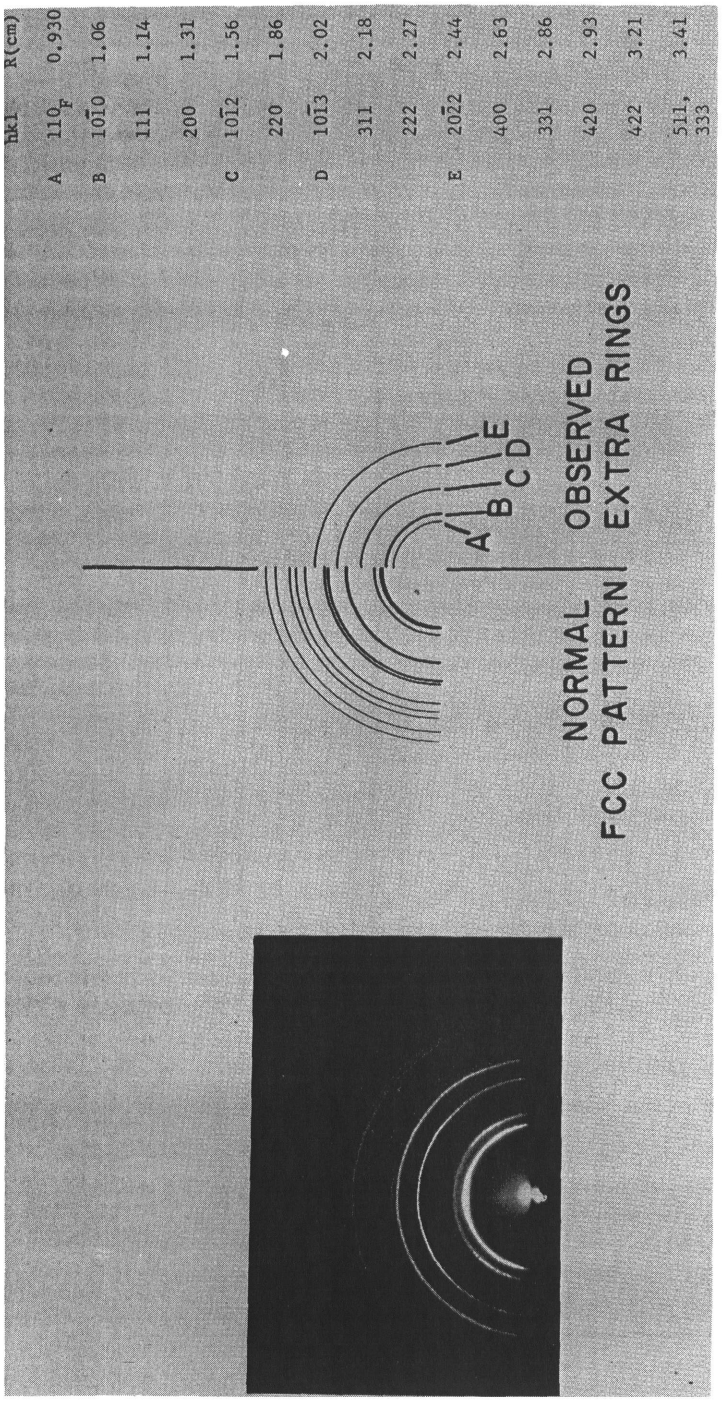

Fig. 1 - Typical reflection diffraction pattern from gold films deposited at substrate temperatures between 375° and 500°C. The line drawing shows the customary fcc reflections and also the extra reflections observed in the diffraction pattern. The accompanying list shows all reflections observed in the pattern and their ring radii.

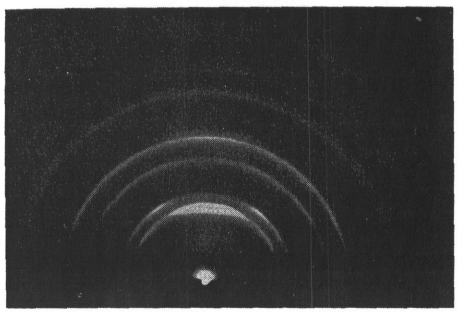

a. Gold film deposited at substrate temperatures below 70°C

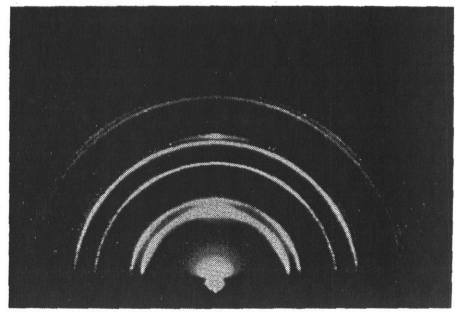

b. Gold film deposited above 650° C

Fig. 2 - Typical reflection diffraction patterns

As discussed previously, a gold film, evaporated onto an optically flat quartz substrate and subsequently melted and annealed, was used as an absolute standard for the machine and for all other measurements on the hot-deposited gold films. Under optimum alignment conditions, such gold-film standards (three were employed and cross-checked against one another) agreed with calculated Bragg-line positions to within ±0.01 degree in 2θ. (It is to be noted that even if the machine alignment shifts slightly due to temperature, mechanical vibration, etc., experimental Bragg-line positions can always be related to the Bragg-line position of the standards without significant error in the measurement.)

In Fig. 3a the (111), (222), and (333) reflections are shown for one of the gold-film standards. In Fig. 3b the (111) reflection for a film deposited at 35°C is shown; no other reflections from this film are observed under the resolution conditions employed. For all the gold films deposited between about 35° and 100°C, the Bragg position for the (111) reflection shifted to higher 2θ values by amounts ranging from 0.02 to 0.04 degree in 2θ; the shift for the 35°C deposit in Fig. 3b is about 0.02 degree. When films deposited at low temperatures are subsequently annealed at temperatures in excess of 400°C but below the melting point, the Bragg lines shifted to higher 2θ values by as much as 0.10 degree for the (111) reflection. Figure 3c shows data for a film which was deposited at 40°C and subsequently annealed at 400°C for one hour without opening the vacuum system; the (111) and (222) reflections have shifted to higher 2θ by 0.08 and 0.19 degree respectively. This type of shift was observed for films which were deposited at low temperatures and subsequently annealed, regardless of whether the film was annealed immediately after the deposition, or first removed from the vacuum system, examined, and then repumped and annealed. Figure 3d shows Bragg-shift data on a film which was deposited at 35°C and then annealed in increasing steps between 400° and 750°C. The data shown are for the film after the 750°C anneal; shifts in 2θ of 0.07 and 0.16 degree are observed for the (111) and (222) reflections, respectively. However, the shift shown in the data occurred with a one-hour anneal at 400°C, and did not change significantly with annealing up to 750°C. As a matter of fact, once the Bragg-line shift was introduced by the annealing at 400° to 500°C, the shift could not be annealed out by sequential annealing up to temperatures as high as 1000°C. Data typical of such behavior are shown in Table 1. In order to anneal out the Bragg-line shift, it was necessary to carry the anneal of the films to the melting point. Such treatment, if carried out for short times, did not cause significant film evaporation, although surface-tension effects caused the film to ball up. It was found that this treatment resulted in complete restoration of the reflections to the theoretical position; the gold-film standard shown in Fig. 3a is a film treated in this manner. The data in Table 1 are typical of such films, from the initial deposit to the final anneal at 1067°C. Three films were treated in this manner; all showed the same behavior, and all recovered to the theoretical Bragg position upon heating to the melting point.

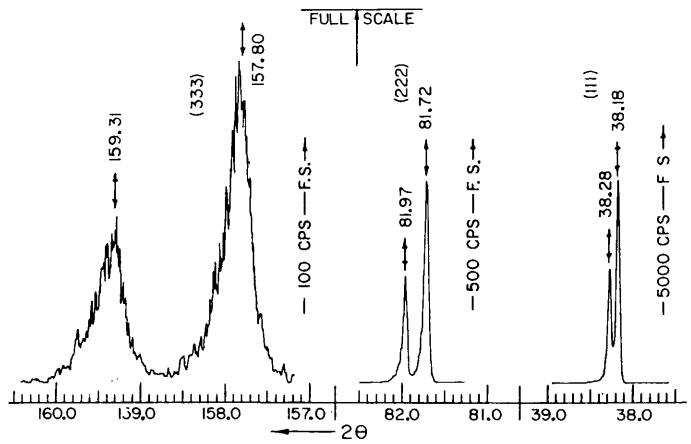

a. The (111), (222), and (333) reflections from a gold film annealed at 1067°C. The 2θ positions agree, to within experimental error, with theory for bulk gold.

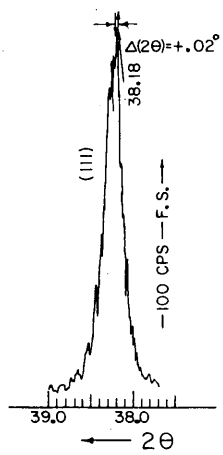

b. The (111) reflection from a gold film deposited at 35°C. The theoretical Bragg position for $CuK\alpha_1$ is at 38.18 and is shown by the arrow pointing upward. The observed α_1 peak is at ~38.20, a shift of ~0.02 degree. Higher-order reflections are not observed from films deposited at 35°C.

c. The (111) and (222) reflections from a film deposited at 40°C and then annealed at 400°C for one hour, without opening the vacuum system. Both of the reflections are well defined and have shifted to higher 2θ values by 0.08 and 0.19 degree, respectively.

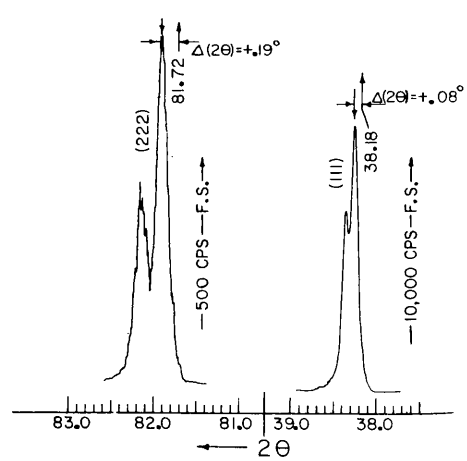

Fig. 3 - X-ray data obtained at a scan of 0.2 °/min with 0.4 MR-HR-0.2° slits. Theoretical Bragg positions are indicated by arrows pointing up, and observed positions by arrows pointing down.

d. The (111) and (222) reflections from a film deposited at 35 °C and then repeatedly annealed at various temperatures (see text) up to 750 °C. The (111) and (222) reflections remain shifted to higher 2θ values with such annealing; the shifts are unaffected by short-term annealing unless the film is heated to the melting point.

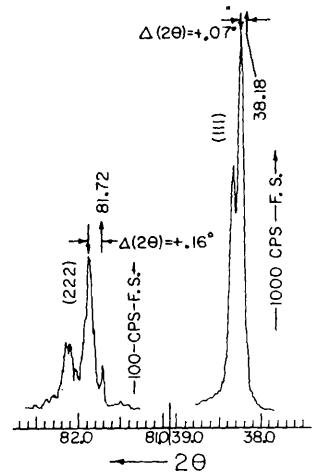

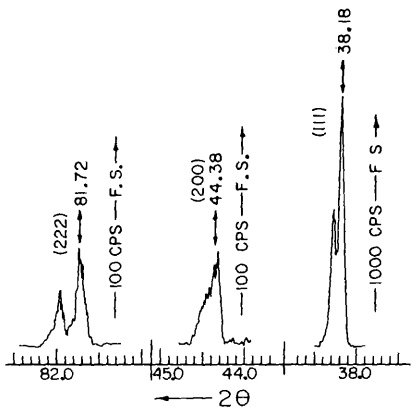

e. The (111), (200), and (222) reflections from a film deposited at 620 °C. Only for films deposited above this temperature does the (200) reflection appear. Films deposited at and above 620 °C exhibit no Bragg shift.

Fig. 3 (Cont'd) - X-ray data obtained at a scan of 0.2°/min with 0.4 MR-HR-0.2° slits. Theoretical Bragg positions are indicated by arrows pointing up, and observed positions by arrows pointing down.

While the shift behavior described occurs for films which are deposited cold, those that are deposited at high temperatures show Bragg-line positions characteristic of the bulk. In general, x-ray measurements on hot-deposited films agree qualitatively with the reflection-electron-diffraction observations, with these exceptions: (a) in no cases were the hexagonally indexed lines or the forbidden (110) observed by x ray; (b) only the (111), (222), and (333) x-ray reflections occurred for depositions up to temperatures of 500 °C. For films deposited at and above 500°C, x-ray data showed a weak (200) reflection whose intensity increased with increasing deposition temperature. Figure 3e shows x-ray data typical of deposition above 500 °C. This particular set of data is for a film deposited at 620 °C; the positions of the reflections agree with theory for bulk gold. The appearance of the (200) for high-temperature deposition is in qualitative agreement with the reflection-electron data, since both exhibit a weakening of the [111] texture toward powder character as the deposition temperature is increased above about 600°C.

Although it can be expected that films deposited cold will contain much higher concentrations of lattice defects of all types, this does not rule out the possibility that the observed Bragg shift could be related to expansion-coefficient mismatch, causing different degrees

Table 1
Bragg-Line Shift for a Typical Cold-Deposited and Annealed Au Film
(0.4 MR-HR-0.02-Degree Slits, Cu Target, Ni Filter)

Treatment	Reflections (degrees)					
	111	$\Delta(2\theta)_{111}$	222	$\Delta(2\theta)_{222}$	333	$\Delta(2\theta)_{333}$
Deposit at 40°C	38.21	+0.03	–	–	–	–
Anneal at 550°C for 1 hr	38.28	+0.10	82.02	+0.30	159.96	+2.16
Anneal at 700°C for 1 hr	38.30	+0.12	82.05	+0.33	160.16	+2.36
Anneal at 720°C for 0.5 hr	38.29	+0.11	82.05	+0.33	160.16	+2.36
Anneal at 720°C for 1.5 hr	38.28	+0.10	82.05	+0.33	160.16	+2.36
Anneal at 770°C for 0.5 hr	38.29	+0.11	82.05	+0.33	160.16	+2.36
Anneal at 850°C for 0.5 hr	38.29	+0.11	82.05	+0.33	160.16	+2.36
Anneal at 1000°C for 10 min	38.30	+0.12	82.07	+0.35	160.18	+2.38
Anneal at 1067°C for 5 min	38.17	-0.01	81.72	±0.00	157.83	+0.03

Note - The dashes indicate reflections which do not appear.

of lattice strain between cold-deposited and hot-deposited films. To eliminate this possibility, films were deposited simultaneously onto substrates with different expansion coefficients, for both cold and hot cases, and then some of the annealing processes described above were carried out. For none of the substrates described above could any correlation be found between expansion-coefficient mismatch and the Bragg shifts observed. In addition, the effects were observed to be independent of evaporation rate, of the boat material, and of thickness.

Resistivity Measurements

Four-probe resistivity measurements were carried out on films over the entire temperature range of deposition. All resistivity measurements were made at room temperature; typical data for films immediately after removal from the vacuum system (no annealing) are given in Table 2. In data of this type the accuracy and precision of the resistivity measurement are limited by the thickness measurement. The method of film-thickness measurement described above usually provides a determination to within ±5 percent for highly reflecting films. However, as can be seen from the table, very high resistivity values are observed for depositions above 500°C, and while film agglomeration has not been observed at these temperatures by optical microscopy, the matte character of the surface introduces uncertainties in the thickness measurement, which makes possible only qualitative comparison with structural and resistivity variations for bulk gold. However, it can be seen from the data that for temperatures below about 100°C, film resistivity can be nearly three times as high as bulk values (column 4, Table 2), while bulk behavior is approached for temperatures exceeding 250°C, finally comparing well with bulk values for deposition between

Table 2
Resistivity Measurements on Unannealed Films
$\rho_{bulk} = 2.4 \times 10^{-6}$

Deposition Temp. (°C)	Thickness (Å)	Measured Resistivity of Film (ρ)	$\frac{\rho}{\rho_{bulk}}$
36	2160	6.3×10^{-6}	2.6
45	3600	5.7×10^{-6}	2.4
60	1100	3.6×10^{-6}	1.5
70	3000	3.3×10^{-6}	1.4
150	1700	3.1×10^{-6}	1.3
200	695	3.0×10^{-6}	1.3
255	2700	2.7×10^{-6}	1.1
275	750	2.6×10^{-6}	1.1
357	4300	2.4×10^{-6}	1.0
380	1350	2.9×10^{-6}	1.2
500	3000	2.5×10^{-6}	1.0
620	2800	1.0×10^{-5}	4.2
720	4300	2.5×10^{-4}	100.

350° and 500°C. Above 600 °C gross deviations from bulk behavior occur; it is to be noted that the matte surface discussed above becomes quite marked in this temperature range.

DISCUSSION

It appears that the extra reflections in the reflection-electron patterns can be attributed either to a real hexagonal close-packed phase or to an apparent hcp phase associated with faulting or twinning. Pashley and Stowell (9) have concluded that all apparent hcp reflections can be explained either by direct diffraction from lattices twinned on {111} planes of the matrix, or by double diffraction involving the matrix and one of the twins. But the absence of certain reflections predicted on this basis seems to indicate that this analysis does not apply to the present work.

According to Pashley and Stowell, direct diffraction from the material in twin orientation, without participation by the matrix, produces extra points in the reciprocal lattice, according to the rule: if $hu + kv + \ell w = 3N \pm 1$, where (uvw) is an allowed matrix reflection, $(hk\ell)$ is the twin plane (of the form {111}), and N is an integer, then $(uvw) \pm (1/3)(hk\ell)$ is allowed. These reciprocal lattice points fall at the same distance from the origin as allowed matrix reflections (since they are in the last analysis merely fcc reflections) and are thus indistinguishable in a powder pattern.

However, when the double-diffraction hypothesis is added to the above mechanism, all points of the form $(uvw) \pm (1/3)(hk\ell)$ appear in the reciprocal lattice. This diffraction occurs in the vicinity of a twin boundary, when a diffracted ray from the matrix (or twin) is rediffracted by the twin (or matrix). The following rule holds for the possibility of these reflections: the reflection $(uvw) \pm (1/3)(hk\ell)$ will appear if in the reciprocal lattice

both this point and the point (abc) fall on the sphere of reflection, (abc) being an allowed reflection in the matrix (or twin), and if the reflection (uvw) ± (1/3) (hkℓ) - (abc) is allowed in the twin (or matrix). The latter need not lie on the sphere of reflection (but will in general in the case of electrons, where the sphere is approximately a plane).

To illustrate, consider the two reflections called (111)⁻ in Ref. 9; their equivalent cubic indices (i.e., having the same radii) are of the forms (a) (1/3) {224} and (b) (1/3) {222}. Reflection a appears, for instance, as the result of the reaction (1/3) (224) = (1/3) (557) + $(\bar{1}\bar{1}\bar{1})$; (1/3) (557) is an allowed twin reflection with a radius equal to that of (311). In the case of reflection b, for instance, (1/3) (222) = (1/3) (228) + $(00\bar{2})$; (1/3) (228) is a twin reflection similar to (220). So in the former case, in order for reflection a to appear, the sphere of reflection (a plane passing through the origin) must intersect simultaneously the point (1/3) (224) and either (1/3) (557) or $(\bar{1}\bar{1}\bar{1})$; similar relations hold for other reflections of the form (1/3) {224}. For b to appear, the sphere must intersect (1/3) (222) and either (1/3) (228) or $(00\bar{2})$; similar requirements hold for other (1/3) {222} reflections. Figure 4 exhibits a portion of the reciprocal lattice (with only the points concerned indicated), and shows that the points (1/3) (557) and $(\bar{1}\bar{1}\bar{1})$ are relatively close to the axis through the origin and (1/3) (224), as compared with the distance of (1/3) (228) and $(00\bar{2})$ from the origin-(1/3) (222) axis. Thus, when the spots have finite extent, as expected from particle size, strains, etc., it may be expected that in a powder pattern a higher proportion of crystallites will satisfy the conditions for diffraction in the (1/3) (224) case than in the (1/3) (222) case; i.e., the former reflection will have a higher intensity than the latter. Indeed, in Fig. 5 of Ref. 9 the (1/3) (224) ring appears quite weakly, and the (1/3) (222) not at all.

It is pointed out by Pashley and Stowell in Ref. 9 that the absence of lines explicable by the double-diffraction hypothesis would provide evidence against it; in the present work no lines have been observed which are derivable from double diffraction but which cannot also be explained by an hcp phase. In particular, the (1/3) (222) ring was not seen. The (1/3) (224) was, but this ring can also be indexed as the hexagonal $(10\bar{1}0)$.

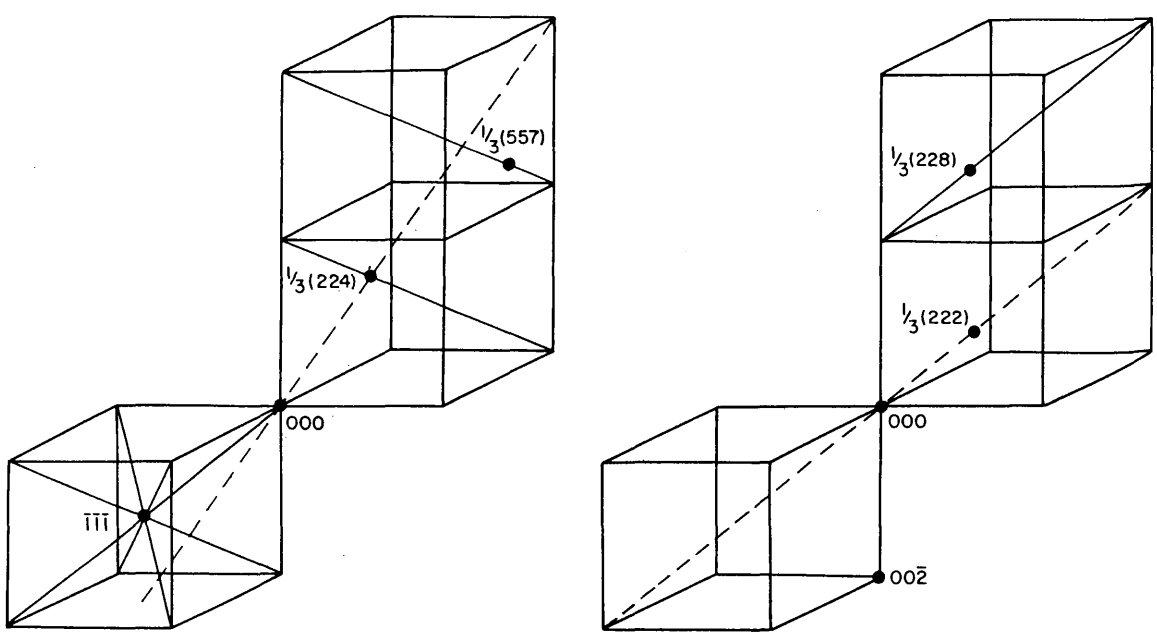

Fig. 4 - Portion of the reciprocal lattice, illustrating how (224) and (222) reflections arise from double diffraction

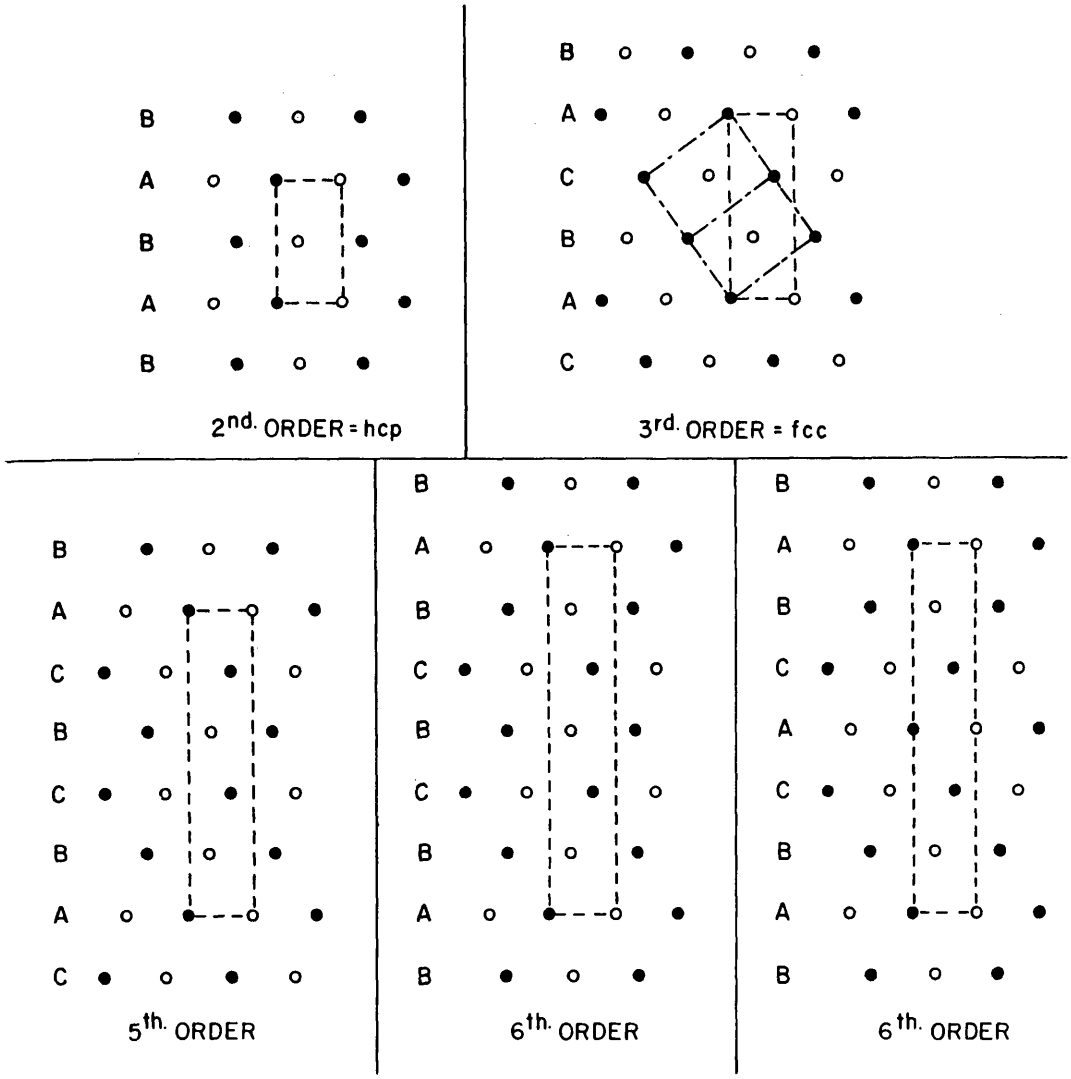

Fig. 5 - Close-packed structures.

● Points in plane of page and at distances $N \frac{a_0}{\sqrt{2}}$ above or below.

o Points at distances $\left(N + \frac{1}{2}\right)\frac{a_0}{\sqrt{2}}$ above or below plane of page.

The quantity a_0 is the cubic lattice constant.

Another ring mentioned in Ref. 9 as evidence for double diffraction is that indexed $(220)^+$ $(222)^-$, with equivalent cubic indices (1/3) (662); this ring should appear immediately outside the (220) ring. In the present work this reflection has been detected, but not without ambiguity. It is not fully resolved from (220), but appears as a fringe on the outside of the latter ring. In many cases there appears to be a symmetrically-placed fringe on the inside which cannot be identified with any predicted reflection; perhaps the explanation for this lies only in dynamical effects. Thus this questionable ring cannot be taken as substantial evidence for the double-diffraction mechanism. Finally, it should be noted that the $(111)^+$, $(222)^+$ $(400)^-$, and $(311)^+$ $(331)^-$ rings, predicted in Ref. 9, were not seen at all.

The Pashley and Stowell paper also discusses several other factors which lead the present authors to doubt that double diffraction is operating in this case. For instance, there is the film buckling mentioned in the Introduction to the present report; both in Refs. 6 and 9 it is stated that the curling and buckling of the film as it is removed from the substrate and placed on a grid form a necessary condition for making double diffraction possible. This is because only such buckling will enable the sphere of reflection to intersect both of the necessary spots – primary and resultant. The films examined here exhibit no such buckling; thus it would appear that the occurrence of the double-diffraction orientations should be far less likely than in the earlier studies.

In addition, in Ref. 9 the authors express uncertainty about the origin of the extra spots in the case of [111] single-crystal gold films; they find ambiguous evidence both for and against the double-diffraction hypothesis. In particular they find that spots of the form (1/3) {224} occur in their electron-diffraction patterns, but the necessary primary spots of form {111} do not. Their conclusion is that these spots arise, not from double diffraction, but from the superlattice of distortions arising at the incoherent boundary between twinned lattices – one of Menzer's (21) proposals (see below). In the present work it is felt that this explanation is also inapplicable, for in these textured-powder patterns such a distortion superlattice should give rise to certain other rings, not indexable hexagonally, which have not been observed. An example of these is the close-together pair (1/3) (533) and (1/3) (622), which might be expected to merge into one comparatively strong ring.

A final consideration against the mechanism of Ref. 9 is the $(20\bar{2}3)$ ring. This ring cannot be fitted into the double-diffraction picture, and was not observed by Pashley and Stowell. These authors suggest that the identification of $(20\bar{2}3)$ by Hirsch, et al. (2) was an erroneous interpretation of random grain-boundary diffraction spots. But in the present work the $(20\bar{2}3)$ ring has been seen in a few films. Its identification has been uncertain, and thus it has not been included in Fig. 1. But if it is present, it is definitely a ring and not just random spots.

The considerations of the above paragraphs lead the authors to favor the conclusion of Hirsch, et al. (2) and of Bahadur and Sastry (3) that the extra reflections in the present work (except for the innermost) arise from a real or apparent hexagonal phase.

Menzer (21) and Göttsche (22) have given comprehensive treatments of twinning phenomena in fcc crystals. Menzer's early work refers to the possibility of "higher-order close-packing" and to lattice distortions which occur at the boundary of two regions twinned on different {111} planes of the matrix. Göttsche proposes "lattice faults of the first and second kinds;" the first kind refers to the misfit of adjacent growth of hcp and fcc lattices, the second to that of two out-of-register hcp lattices.

Menzer's higher-order close-packing is a development of the normal hcp and fcc sequences of close-packed atomic planes. If A, B, and C represent the three possible positions of the close-packed planes with respect to a line normal to them, the hcp structure arises from a stacking sequence ...ABABAB..., which may be called second order; the third-order sequence ...ABCABC... produces the fcc structure in (111) orientation. Figure 5 shows these structures with the hexagonal unit cells outlined; in the third-order case the cubic unit cell is also outlined. The a axes of the hexagonal cells come perpendicularly out of the page; the b axes point to the right and into the page at an angle of 30 degrees. Of interest here are the fifth-order stacking ...ABCBC... and the two possible sixth-order sequences ...ABCBCB... and ...ABCACB..., also shown in Fig. 5. This is because the innermost reflection, A of Fig. 1, the ratio of whose radius to that of the (111) ring is $R/R_{111} = 0.82$, can be approximately fitted to the (0004) reflection of a fifth-order structure, $R/R_{111} = 4/5$, or to the (0005) reflection of either sixth order, $R/R_{111} = 5/6$. But even ignoring the comments by Menzer on the improbability of such

higher-order close-packing sequences, a structure-factor calculation quickly shows that (0004) in fifth-order stacking, and (0005) in either sixth-order sequence, are forbidden reflections. Thus, this possibility should be ruled out as an explanation for the inner ring.

Menzer also considers two lattices which arise from the same matrix by twinning on different {111} planes, and the distortions occurring in the boundary region between them. He finds that the extra points contributed to the reciprocal lattice by these distortions are of the family $(u \pm 1/3, v \pm 1/3, w \pm 1/3)$; i.e., the same points considered much later by Pashley and Stowell (9).

Göttsche's analysis likewise does not lead to any reflections different from those considered above. He considers reflections arising from superlattices of faults generated by (a) adjacent growth of hcp and fcc phases, or (b) adjacent growth of two non-coincident hcp structures (e.g., ...ABAB... and ...ACAC...). These reflections, together with the normal hcp, again lead to spots of the family $(u \pm 1/3, v \pm 1/3, w \pm 1/3)$.

None of these analyses provides an explanation of the ring at $R/R_{111} = 0.82$. The authors are left with the interpretation of it as the forbidden (110) reflection, arising either from relaxation effects associated with small crystallite size or with vacancy concentrations, or from a process such as the "systematic interaction" explained by Hoerni (23) and invoked by Takagi and Morimoto (24) to explain the forbidden (222) reflection in germanium.

One explanation which could be introduced (25) assumes that there are some crystallites thin enough in a [001] direction (only a few atomic layers) that the (111) reciprocal lattice point may be stretched out to intercept the (001) reciprocal lattice plane in a (110) position. However, this implies that in a powder pattern the sphere of reflection would intersect this "spike" in many places, and thus that a continuous band should appear between the (110) and (111) rings. This explanation, then, can be offered only for extra spots in a single-crystal pattern.

There remain two possibilities for this (110) reflection. The first is modification of the structure factor due to large concentrations of lattice vacancies; further evidence for this is adduced later in this report. The other is the "systematic interaction" process, which depends on the planarity of the sphere of reflection in the electron case; if any of the points $\pm(uvw)$, $\pm(2u, 2v, 2w)$, $\pm(3u, 3v, 3w)$, ... are located on the sphere of reflection, all are, and if one of these corresponds to an allowed reflection, others can arise due to dynamical interaction. Thus, in the present case (220) gives rise to (110).

The presence of the hexagonally indexed lines (B through E in Fig. 1) can be attributed either to a real hcp phase or to an apparent hcp structure arising from a high concentration of randomly repeated faulting or twinning. Hirsch, et al. (2) comment that the latter phenomenon would give rise only to lines of the form $h - k \neq 3N$, ℓ odd; the presence of the lines $(10\bar{1}0)$, $(10\bar{1}2)$, $(20\bar{2}2)$ contradicts this. Moreover, although the stacking-fault hypothesis is also suggested by the deviations of resistivity of the films deposited at low and high temperatures, which might be due to scattering, this consideration can be shown to be untenable. Cotterill (18) finds the resistivity introduced into a gold sample by a concentration β cm^{-1} of stacking faults to be

$$\rho_{sf} = 1.8 \times 10^{-13} \beta \text{ ohm-cm}^2$$

The author defines $\beta = \sqrt{3}\, L^2 C_t$, where C_t is the concentration per unit volume of stacking-fault tetrahedra of root-mean-square edge L. The faulting probability α for a (111)-oriented film is given by the ratio of the total areas of three faces of the tetrahedra to

the total area of the three {111} planes, other than the plane of the film – the three on which faulting occurs. Then if V is the volume of the sample and d the (111) plane spacing,

$$\alpha = \frac{\frac{3}{4}\sqrt{3}\, L^2 C_t V}{3\, V/d} = \frac{\sqrt{3}}{4} L^2 d C_t = \frac{1}{4}\, d\beta$$

and

$$\rho_{sf} = 3.1 \times 10^{-5}\ \alpha \text{ ohm-cm}.$$

In view of the resistivity ratios in Table 2 for the low- and high-temperature depositions, consider a case where the film resistivity is increased by a factor of two over the bulk value at room temperature, which is 2.4×10^{-6} ohm-cm, and assume this increase to be due to stacking faults. Then $\rho_{sf} = 2.4 \times 10^{-6}$ ohm-cm, and $\alpha = 0.08$.

Warren (20) finds that a stacking-fault density α causes a shift in peak position of

$$\Delta(2\theta) = \alpha\, A \tan\theta\ ,$$

where A is a constant, different for each reflection, which is 3.95 degrees for (111) and -1.92 degrees for (222). Then for $CuK\alpha_1$ radiation, $\theta_{111} = 19.09$ degrees and $\theta_{222} = 40.81$ degrees, and the peak shifts are respectively 0.11 and -0.14 degree. Thus, if the resistivity deviations in Table 2 were due to stacking faults, a large line shift would occur in such a way as to decrease the separation between (111) and (222); no such shift has been observed. Thus, it appears that a true hexagonal phase exists in the authors' films.

On the other hand, where a shift occurred, all peaks moved to higher Bragg angles (Fig. 1 and Table 1); moreover, in all cases the shift in 2θ increased with increasing 2θ. If one assumes these shifts to be due to a real contraction of the lattice, one has from the Bragg law

$$\cot\theta\, \Delta(2\theta) = \text{constant}\ .$$

For $CuK\alpha_1$ radiation, the shifts in the (111), (222), and (333) reflections are in the ratio 1:2.5:15. A compilation of typical shift data from various films is given in Table 3; the data in this table give reasonable agreement with the above ratios, especially in the cases where all the peaks are well defined.

Lattice-contraction effects have also been observed for vacuum-deposited films of nickel and copper by Suhrmann, et al. (14); they found similar shifts to higher 2θ, which increased with 2θ in about the same manner as observed in the present work. In an investigation of the quenching-in of vacancies in copper, silver, and gold subjected to spark discharge, Palatnik and Levechenko (12) found significant decreases in lattice constant. They eliminated both stress effects and the formation of solid solutions as contributory, and deduced that the lattice contraction was due to large concentration of vacancies introduced during the spark. In a later, related work Palatnik and Il'inskii (13) interpreted shifts of x-ray reflections for copper and silver as due to a lattice contraction associated with vacancies inherent in the vacuum-deposition process; those results also are in substantial agreement with the present observations on fold films.

In 1958, Tewordt (26) calculated lattice-distortion effects around various defects in copper and other fcc metals; in addition, that paper gives an excellent review of all of the techniques involved in these calculations. Thus, in a later paper (27) Bennemann and Tewordt found a lattice expansion in the case of interstitials in copper and a lattice contraction in the case of vacancies in copper; they also indicate that the same behavior is to be expected for gold.

Table 3
Bragg Shift with Annealing of
Cold-Deposited Gold Films

Anneal Temperature (°C)	Reflections		
	$\Delta(2\theta)_{111}$	$\Delta(2\theta)_{222}$	$\Delta(2\theta)_{333}$
550*	0.06	0.12	-
550†	0.09	0.25	-
No anneal	0.02	-	-
No anneal	0.03	0.09	-
700	0.08	0.25	-
550	0.06	0.20	-
500	0.06	0.20	1.51
700	0.11	0.35	2.13
720	0.07	0.25	-
400	0.08	-	-
400‡	0.04	0.26	1.82
400‡	0.11	0.29	2.03
560	0.04	0.13	1.30
740	0.08	0.23	1.65

*Au on C on mica.
†Au on C on SiO_2.
‡Samples cold-deposited and annealed before removal from vacuum system.
Note - The dashes indicate reflections which do not appear.

In investigations on fcc metals, Simmons and Balluffi (28-31) have related dilation measurements to quenched-in vacancies and their annealing properties. Similarly, the quenched-in electrical resistivity of fcc metals has been related to stacking faults and vacancies, both by indirect measurements and direct observation in the electron microscope; these effects have been treated theoretically by a number of authors. For instance, de Jong and Koehler (32) have treated experimentally and theoretically the properties of mono-, di-, tri-, and tetravacancies in quenched gold; in all cases vacancies anneal out at temperatures well below the melting point. In the present work, however, the defects which were quenched into the lattice by the very nature of the cold-deposition process did not anneal out unless the films were heated to the melting point (Fig. 3 and Table 1). By virtue of the fact that the Bragg-line shift is in the direction of a lattice contraction, the authors identify the defects as vacancies, in agreement with other work listed above. However, in view of the discrepancies between the annealing behavior of these films and of bulk gold, the authors must assume that the vacancies form very stable complexes (of higher order than those reported by de Jong and Koehler) when a cold-deposited film is annealed to above 350°C; these complexes do not dissociate and/or diffuse out with short anneals at temperatures as high as 1000°C, but x-ray examination of such films after heating to just above the melting point shows complete return to bulk behavior.

ACKNOWLEDGMENT

The authors would like to thank Dr. D. W. Pashley of Tube Investments Research Labs., Hinxton Hall, Essex, England, for helpful criticism and commentary on the work.

REFERENCES

1. Finch, G.I., Quarrell, A.G., and Wilman, H., Trans. Faraday Soc. 31:1051 (1935)
2. Hirsch, P.B., Kelly, A., and Menter, J.W., Proc. Phys. Soc. (London) B. 68:1132 (1955)
3. Bahadur, K., and Sastry, P.V., Proc. Phys. Soc. (London) 78:594 (1961)
4. Ogawa, S., Watanabe, D., and Fujita, F.E., J. Phys. Soc. Japan 10:429 (1955)
5. Rüdiger, O., Ann. Physik 30:519 (1937)
6. Brück, L., Ann. Physik 26:233 (1936)
7. Goche, O., and Wilman, H., Proc. Phys. Soc. (London) 51:625 (1939)
8. Burbank, R.D., and Heidenreich, R.D., Phil. Mag. 5:373 (1960)
9. Pashley, D.W., and Stowell, M.J., Phil. Mag. 8:1605 (1963)
10. Parker, R.L., and Krinsky, A., J. Appl. Phys. 34:2700 (1963)
11. Catlin, A., and Walker, W.P., J. Appl. Phys. 31:2135 (1960)
12. Palatnik, L.S., and Levchenko, A.A., Soviet Phys. Solid State 3:2556 (1962)
13. Palatnik, L.S., and Il'inskii, A.I., Soviet Phys. Solid State 4:2609 (1963)
14. Suhrmann, R., Wedler, G., Wilke, H.G., and Reusmann, G., Z. physik. Chem. 26:85 (1960)
15. Heavens, O.S., Proc. Phys. Soc. (London) 65B:788 (1952)
16. Davey, J.E., and Deiter, R.H., Phys. and Chem. Glasses 4:213 (1963)
17. Haseyawa, Y., and Kawakubo, S., J. Spectrom. Soc. Japan 11:245 (1963)
18. Cotterill, R.M.J., Phil. Mag. 6:1351 (1961)
19. Statz, H., Z Naturforsch. 17a, #11:994 (1962)
20. Warren, B.E., Progr. in Metal Phys. 8:147 (1959)
21. Menzer, G., Z. Krist. 99:378 (1938)
22. Göttsche, H., Z. Physik 134:517 (1953)
23. Hoerni, J.A., Phys. Rev. 102:1534 (1956)
24. Takagi, M., and Morimoto, S., J. Phys. Soc. Japan 18:819 (1963)
25. Pinsker, Z.G., "Electron Diffraction," London:Butterworths Scientific Publications, p. 88, 1953
26. Tewordt, L., Phys. Rev. 109:61 (1958)
27. Bennemann, K.H., and Tewordt, L., Z. Naturforsch. 15a:772 (1960)
28. Simmons, R.O., and Balluffi, R.W., Phys. Rev. 117:52 (1960)
29. Simmons, R.O., and Balluffi, R.W., Phys. Rev. 119:600 (1960)
30. Balluffi, R.W., and Simmons, R.O., J. Appl. Phys. 31:2284 (1960)
31. Simmons, R.O., and Balluffi, R.W., Phys. Rev. 125:862 (1962)
32. de Jong, M., and Koehler, J.S., Phys. Rev. 129:40 (1963)